



Retinal inputs signal astrocytes to recruit interneurons into visual thalamus

Jianmin Su^{a,1}, Naomi E. Charalambakis^{b,1}, Ubadah Sabbagh^{a,c} , Rachana D. Somaiya^{a,c}, Aboozar Monavarfeshani^{a,d}, William Guido^{b,2}, and Michael A. Fox^{a,d,e,2}

^aCenter for Neurobiology Research, Fralin Biomedical Research Institute at Virginia Tech Carilion, Roanoke, VA 24016; ^bDepartment of Anatomical Sciences and Neurobiology, University of Louisville School of Medicine, Louisville, KY 40202; ^cGraduate Program in Translational Biology, Medicine, and Health, Virginia Tech, Blacksburg, VA 24061; ^dDepartment of Biological Sciences, Virginia Tech, Blacksburg, VA 24061; and ^eDepartment of Pediatrics, Virginia Tech Carilion School of Medicine, Roanoke, VA 24016

Edited by Carol Ann Mason, Columbia University, New York, NY, and approved December 24, 2019 (received for review July 29, 2019)

Inhibitory interneurons comprise a fraction of the total neurons in the visual thalamus but are essential for sharpening receptive field properties and improving contrast-gain of retinogeniculate transmission. During early development, these interneurons undergo long-range migration from germinal zones, a process regulated by the innervation of the visual thalamus by retinal ganglion cells. Here, using transcriptomic approaches, we identified a motogenic cue, fibroblast growth factor 15 (FGF15), whose expression in the visual thalamus is regulated by retinal input. Targeted deletion of functional FGF15 in mice led to a reduction in thalamic GABAergic interneurons similar to that observed in the absence of retinal input. This loss may be attributed, at least in part, to misrouting of interneurons into nonvisual thalamic nuclei. Unexpectedly, expression analysis revealed that FGF15 is generated by thalamic astrocytes and not retino-recipient neurons. Thus, these data show that retinal inputs signal through astrocytes to direct the long-range recruitment of interneurons into the visual thalamus.

astrocyte | thalamus | interneuron

Local GABAergic interneurons comprise only a fraction of the total neurons in the mammalian brain but are essential for controlling the spatial and temporal spread of excitatory activity. The development of these inhibitory interneurons, and their incorporation into neural circuits, is a protracted process that includes both cell-autonomous mechanisms for the acquisition of cell-type specification and noncell-autonomous ones for the regulation of their recruitment and circuit assembly (1, 2). While mechanisms underlying these processes have been studied extensively in the neocortex (3), they remain poorly understood in the visual thalamus. In rodents, the primary retinorecipient regions of visual thalamus include the dorsal lateral geniculate nucleus (dLGN), ventral LGN (vLGN), and intergeniculate leaflet (IGL). These nuclei receive input from a highly diverse group of retinal ganglion cells (RGCs) but only the dLGN serves as a relay of retinal information to the visual cortex (4–6). Unlike many other regions of rodent thalamus, these three nuclei each contain local GABAergic interneurons (6–8).

The dLGN, similar to the neocortex, contains a small percentage (10 to 20%) of GABAergic interneurons (8–10). In contrast to the great diversity of interneuron subtypes in the neocortex (1), dLGN interneurons are homogeneous, clustering into just one or two subtypes based on morphology, intrinsic membrane properties, gene expression, and embryonic origin (11–14). GABAergic interneurons in dLGN receive monosynaptic input from RGCs and provide feedforward inhibition onto excitatory thalamocortical relay cells (15–17). Such input serves to sharpen receptive field properties and improve the contrast-gain of retinogeniculate transmission (17–20). In contrast to the dLGN (and neocortex), a significantly higher fraction of cells in the vLGN and IGL are GABAergic (6, 21–24). The connectivity and function of these GABAergic neurons remains unclear; however, they appear to represent a heterogeneous

collection of cell types based on their distribution, gene and neurochemical expression, and projection patterns (5–7, 25).

Despite the presence of GABAergic interneurons in the visual thalamus of the adult mouse, these cells are largely absent at birth when RGC axons innervate these nuclei (12). Also lacking from the visual thalamus at these early ages are nonretinal inputs that arise from the neocortex, brainstem, and the thalamic reticular nucleus. Indeed, these inputs comprise ~90% of the afferents to these retinorecipient regions in adults (16, 26, 27). A number of recent studies revealed that retinal innervation plays an instructive role in the recruitment of nonretinal inputs into the visual thalamus (28–30). Retinal input has also been implicated in controlling the spatial distribution of interneurons within the dLGN (12). Here, we used a genetic model that fails to generate connections between the retina and brain (31, 32) to demonstrate that, in the absence of retinal input, fewer GABAergic interneurons are recruited into the visual thalamus. Using transcriptomic approaches, we sought to understand the mechanisms underlying retinal input-regulated interneuron recruitment and identified fibroblast growth factor 15 (FGF15) as a candidate motogenic cue whose expression in the visual thalamus is controlled by retinal innervation. Loss of this FGF results in impaired migration of GABAergic interneurons into the dLGN and vLGN. Surprisingly, we discovered that this FGF is

Significance

Local inhibition, mediated by thalamic interneurons, contributes to the processing of visual information and is essential for vision. However, the mechanisms underlying the development of these interneurons remains unresolved. In this study, we sought to identify mechanisms that contribute to the long-distance migration of these interneurons into the visual thalamus. Our data show that innervation of the visual thalamus by retinal ganglion cells, the output neurons of the retina, is necessary for normal interneuron migration. Surprisingly, axons from these retinal ganglion cells appear to signal through astrocytes to contribute to thalamic interneuron migration. Astrocyte-derived cues may be a general mechanism for guiding interneuron migration throughout the brain.

Author contributions: J.S., N.E.C., U.S., W.G., and M.A.F. designed research; J.S., N.E.C., U.S., R.D.S., and A.M. performed research; J.S., N.E.C., U.S., R.D.S., A.M., W.G., and M.A.F. analyzed data; and J.S., N.E.C., U.S., W.G., and M.A.F. wrote the paper.

The authors declare no competing interest.

This article is a PNAS Direct Submission.

This open access article is distributed under [Creative Commons Attribution-NonCommercial-NoDerivatives License 4.0 \(CC BY-NC-ND\)](https://creativecommons.org/licenses/by-nc-nd/4.0/).

¹J.S. and N.E.C. contributed equally to this work.

²To whom correspondence may be addressed. Email: william.guido@louisville.edu or mafox1@vtc.vt.edu.

This article contains supporting information online at <https://www.pnas.org/lookup/suppl/doi:10.1073/pnas.1913053117/-DCSupplemental>.

First published January 21, 2020.

generated by thalamic astrocytes, suggesting a mechanism by which retinal inputs signal through astrocytes to induce the recruitment of GABAergic neurons into retinorecipient regions.

Results

Retinal Inputs Are Necessary for Interneuron Recruitment into the Visual Thalamus. To determine how and when GABAergic interneurons populate the main retinorecipient nuclei of the visual thalamus, we utilized a bacterial artificial chromosomal transgenic mouse expressing GFP under control of the *Gad1* promoter (i.e., *Gad67-GFP*), allowing us to track GFP⁺ interneuron migration (*SI Appendix, Fig. S1*) (12, 33, 34). Nearly all interneurons in the dLGN are labeled in *Gad67-GFP* mice and GFP expression can be detected as early as postnatal day 0 (P0) (*SI Appendix, Fig. S1*) (11, 28, 33). A large number of GFP⁺ interneurons are also present in the vLGN of these mice; however, in this region these represent only a fraction of the total GABAergic neurons (*SI Appendix, Fig. S1*). Despite containing GABAergic neurons (*SI Appendix, Fig. S1*) (7, 23), few GFP⁺ cells were detected in the IGL of *Gad67-GFP* mice (*SI Appendix, Fig. S1*). Thus, while *Gad67-GFP* is a faithful reporter line for GABAergic interneurons in the adult dLGN, it labels only a subset of the diverse GABAergic cells in other regions of the visual thalamus.

During early development, the number and distribution of GFP⁺ GABAergic interneurons in these regions differed from the adult profile in several ways. At birth (P0), the large majority of GFP⁺ interneurons in the visual thalamus were found in the vLGN, with just a few observed in the dLGN (Fig. 1A). Over the

first week of postnatal development, this distribution shifted, with the dLGN showing a rapid increase and the vLGN a concomitant decrease in GFP⁺ interneuron number (Fig. 1A, C, and D). Initially, interneurons clustered within the dorsolateral tier of the neonatal dLGN, just beneath the optic tract (Fig. 1A) (12, 35); however, by the end of the first postnatal week GFP⁺ interneurons were dispersed evenly throughout the entire dLGN (Fig. 1A). To track and quantify this progression, we divided the dLGN in half, and quantified GFP⁺ interneuron numbers in the dorsolateral and ventromedial halves to generate a “top-to-bottom” ratio (Fig. 1E). At neonatal ages (P0 to P3), there was a significantly higher ratio (~2:1) of interneurons in the dorsoventral half of the dLGN compared to older ages (Fig. 1E).

These results reveal that the timing of interneuron recruitment and dispersion in the visual thalamus coincides with the refinement of retinogeniculate circuits (4). Moreover, previous studies reported that retinal input directs the spacing and circuit integration of interneurons in the dLGN (12, 35). For these reasons, we asked whether retinal inputs also influence the recruitment of interneurons into the dLGN and vLGN. To address this, we crossed *Gad67-GFP* mice to *Math5*^{-/-} mice, which lack RGCs and their central projections (*SI Appendix, Fig. S1*) (29, 32, 36). Importantly, *Math5* is not generated in the visual thalamus (29, 37–39). Two important differences were observed in the distribution of interneurons in *Gad67-GFP::Math5*^{-/-} and *Gad67-GFP* mice (Fig. 1B and *SI Appendix, Fig. S1*). In the absence of retinal input there was an overall reduction in the number of interneurons found in the vLGN and dLGN (Fig. 1B–D

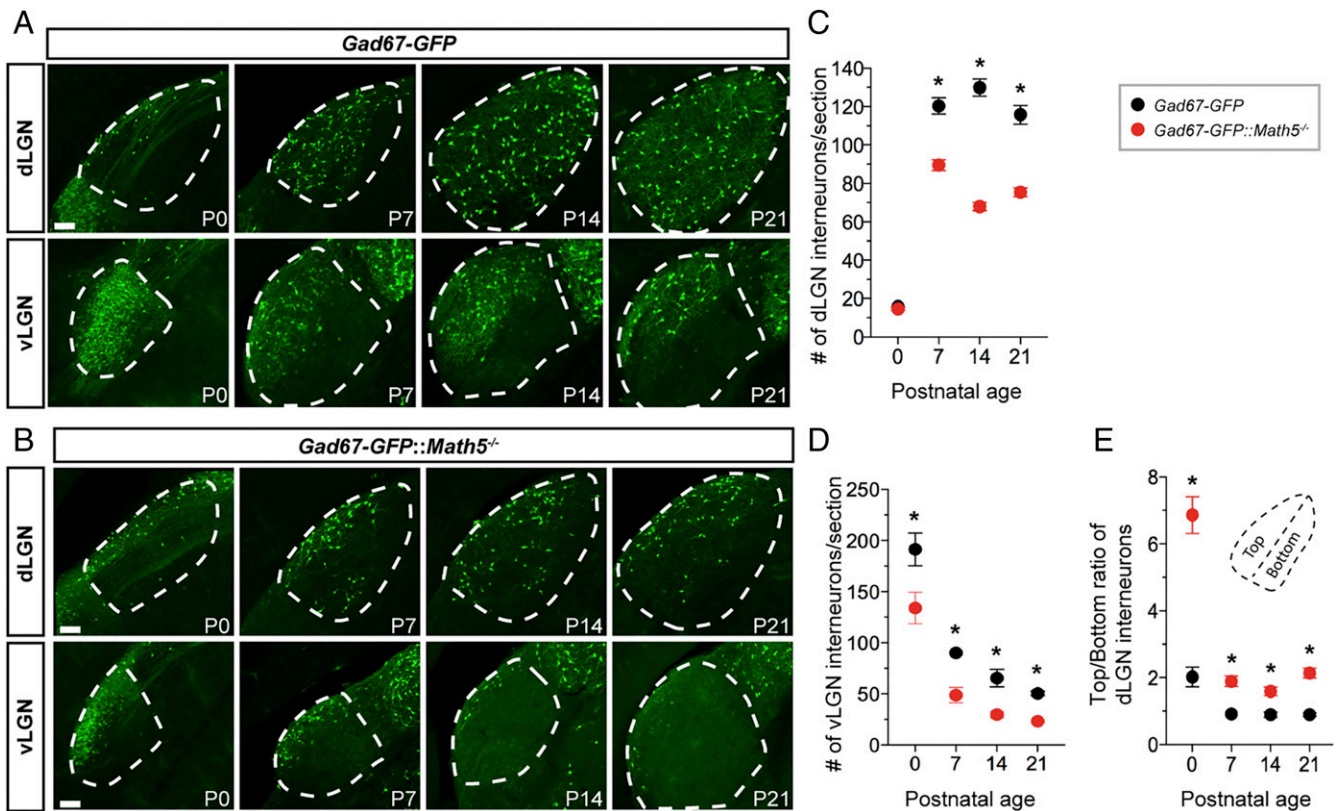


Fig. 1. Retinal inputs are necessary for interneuron recruitment into the visual thalamus. (A and B) GFP⁺ GABAergic interneurons in visual thalamus of P0 to P21 *Gad67-GFP* (A) and *Gad67-GFP::Math5*^{-/-} mice (B). The dLGN and vLGN are highlighted by dashed lines. (Scale bars, 70 μ m.) (C and D) Summary of age-related changes in GFP⁺ interneuron number in the dLGN (C) and vLGN (D) of *Gad67-GFP* and *Gad67-GFP::Math5*^{-/-} mice. Data points represent means \pm SEM. Asterisks (*) represent significance ($P < 0.001$) between control and mutant [two-way ANOVA, $F_{(9, 178)} = 198.2$, $P < 0.001$; Holm-Sidak post hoc test, all P values < 0.0001]. (E) Quantification of interneuron distribution within dLGN of *Gad67-GFP* and *Gad67-GFP::Math5*^{-/-} mice. Dashed line in inset shows the axis used to delineate the dorsolateral half (“Top”) of dLGN from the ventromedial shell (“Bottom”). Data points represent means \pm SEM. Asterisks (*) represent significance ($P < 0.001$) between control and mutant [two-way ANOVA, $F_{(9, 181)} = 53.29$, $P < 0.0001$; Holm-Sidak post hoc test, all P values < 0.0001].

and *SI Appendix, Fig. S2*). Moreover, those remaining in the dLGN were clustered within the dorsolateral tier of the nucleus. At all ages there was a twofold increase in the top-to-bottom ratio of GFP⁺ interneurons in *Gad67-GFP::Math5^{-/-}* mice compared with controls (*Fig. 1E*). Thus, retinal inputs are required for the appropriate migration of interneurons into and throughout the developing visual thalamus.

There are at least two possible mechanisms underlying reduced numbers of interneurons in the *Gad67-GFP::Math5^{-/-}* visual thalamus. The absence of retinal input may trigger programmed cell death in thalamic interneurons or may disrupt the targeting of migrating GFP⁺ interneurons into the visual thalamus. To test for increased cell death, we immunostained sections of the mutant and control visual thalamus with antibodies directed against cleaved caspase 3 (Casp3), a marker of programmed cell death (40). While Casp3⁺ cells were found in the developing visual thalamus of both *Gad67-GFP::Math5^{-/-}* and *Gad67-GFP* mice (as well as in the potential thalamic and tectal migratory paths of thalamic GABAergic interneurons) (12, 13), none appeared to be Casp3⁺/GFP⁺ interneurons (*SI Appendix, Fig. S2*). This observation not only suggests that local interneurons may not undergo developmental programmed cell death in the visual thalamus of *Gad67-GFP* mice, it also ruled out the possibility that reduced numbers of GABAergic interneurons in the visual thalamus of *Gad67-GFP::Math5^{-/-}* mice result from increased programmed cell death.

Next, to test whether interneurons might be misrouted in the absence of retinal input, we examined the distribution of GFP⁺ interneurons in adjacent regions of the dorsal thalamus,

such as the ventrobasal complex (VB), which contains few resident GABAergic interneurons (*SI Appendix, Fig. S1*) (8, 41, 42) and which resides along one of the presumed migratory paths for thalamic interneurons originating from the wall of the third ventricle (12; but see also ref. 13). At birth, few GABAergic interneurons were present in the VB of *Gad67-GFP* mice (*Fig. 2A*), and while the number of interneurons in the VB increased during the first two postnatal weeks, overall the total remained five- to sixfold lower than in the dLGN and vLGN (*Fig. 2C and D*). Increased numbers of GFP⁺ interneurons were present in the VB of *Gad67-GFP::Math5^{-/-}* mutants, starting as early as P7 (*Fig. 2B, C, and E*). We interpret the increased GFP⁺ cells in the nonretino-recipient thalamus to be misrouted interneurons that were bound for the dLGN and vLGN; however, it is possible they came from other sources. To begin to shed light on this issue, we recently identified a gene (*Asic4*) expressed in most, if not all, GABAergic interneurons in the dLGN and a significant fraction of GABAergic cells in the vLGN (*SI Appendix, Fig. S3*). Importantly, this gene is not generated by many GABAergic neurons in other brain regions, including the hippocampus or VB (*SI Appendix, Fig. S3*). However, *Asic4⁺* cells were present in the VB of *Math5^{-/-}* mutants, suggesting that these cells were transcriptionally similar to GABAergic cells in the dLGN and vLGN (*SI Appendix, Fig. S3*). Taking these data together, we interpret these data to suggest that LGN-bound interneurons may become misrouted into inappropriate thalamic nuclei in the absence of retinal input.

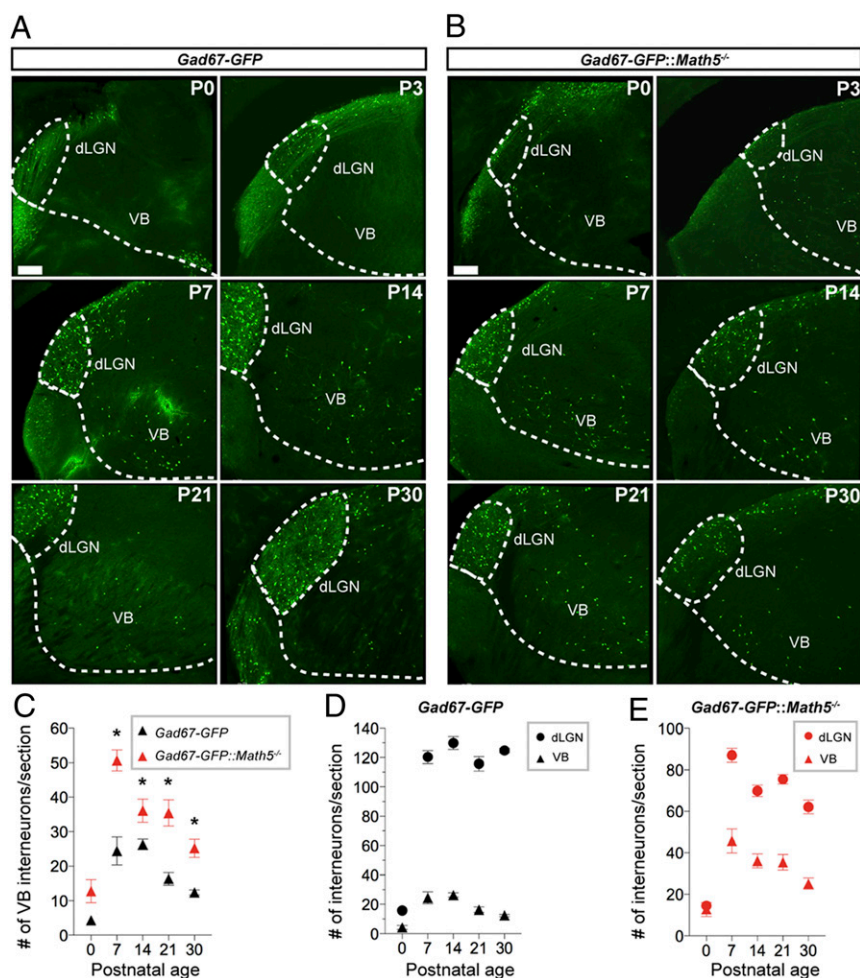


Fig. 2. Increased numbers of interneurons in the VB in the absence of retinal input. (A and B) GFP⁺ GABAergic interneurons in the dorsal thalamus of P0 to P30 *Gad67-GFP* (A) and *Gad67-GFP::Math5^{-/-}* mice (B). (Scale bars, 150 μ m.) (C–E) Summary of age-related changes in GFP⁺ interneuron number in the VB (triangles) and dLGN (circles) of *Gad67-GFP* and *Gad67-GFP::Math5^{-/-}* mice. Data points represent means \pm SEM, Asterisks (*) in C represent significance ($P < 0.001$) between control and mutant [two-way ANOVA, $F_{(1, 134)} = 94.43$, $P < 0.0001$; Holm–Sidak post hoc test, P values < 0.001].

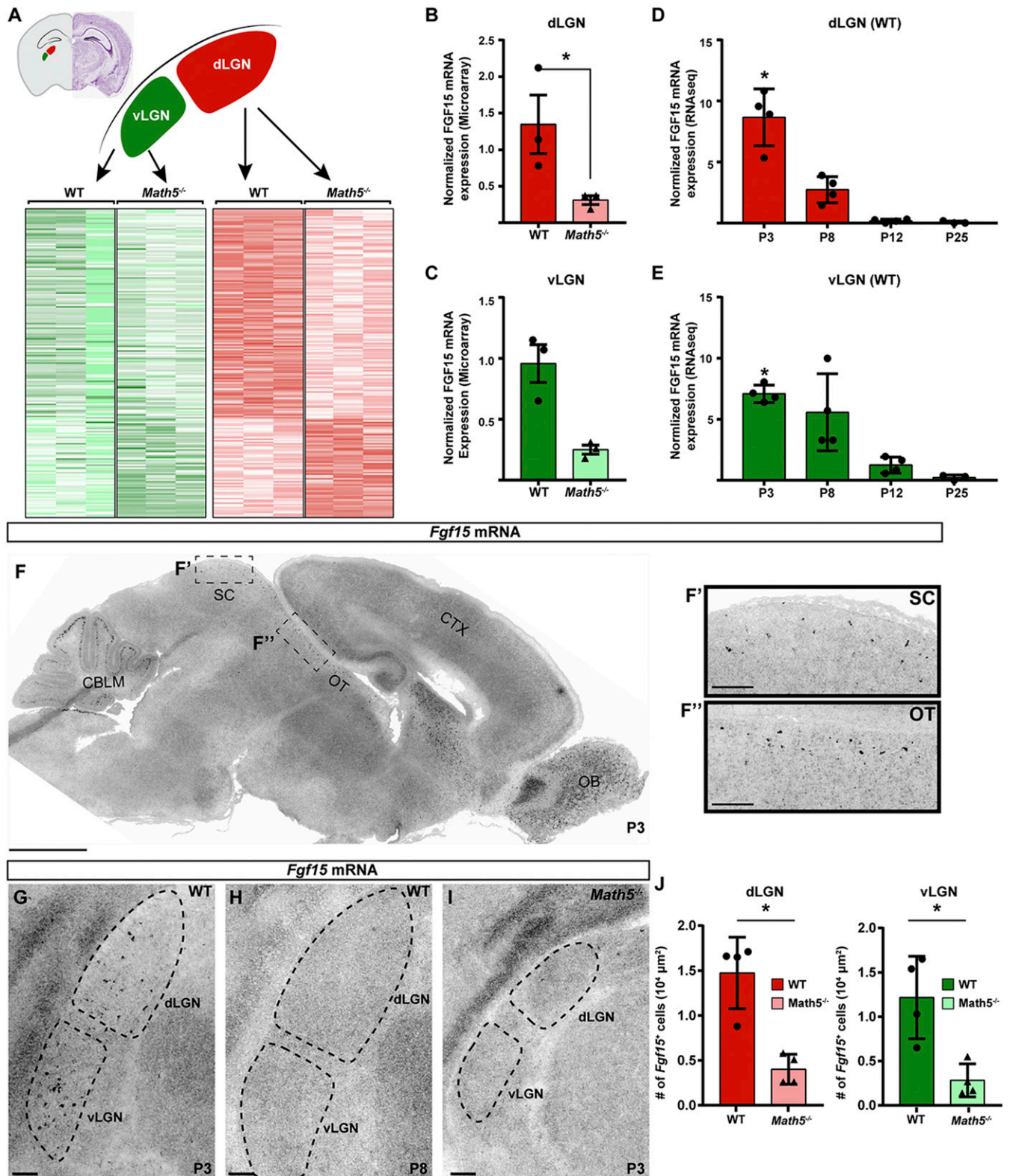


Fig. 3. *Fgf15* expression in the visual thalamus is dependent on retinal input. (A) Heat maps of differential gene expression in P2 WT and *Math5*^{-/-} vLGN and dLGN assessed by Agilent microarrays (full dataset in ref. 29). (B and C) Microarray analysis revealed significant loss of *Fgf15* mRNA expression in the dLGN (B) and vLGN (C) in P2 *Math5*^{-/-} mutants. Bars represent means \pm SEM, Asterisks (*) represent significance ($P < 0.05$) between by two-way ANOVA. (D and E) RNA-seq analysis revealed *Fgf15* mRNA expression decreases postnatally in the WT dLGN (D) and vLGN (E). Bars represent means \pm SEM. Asterisks (*) represent significantly enriched expression at P3 compared to P12 and P25 ($P < 0.05$) by two-way ANOVA. (F–H) ISH revealed *Fgf15* mRNA expression in the SC, optic tract (OT), dLGN, and vLGN at P3 (G), but little to no expression at P8 (H). (I) ISH revealed significantly reduced *Fgf15* mRNA expression in the visual thalamus in P3 *Math5*^{-/-} mutants. (J) *Fgf15*⁺ cells were quantified in the dLGN and vLGN of P3 *Math5*^{-/-} mutants and WT controls. Bars represent means \pm SEM. Asterisks (*) represent significantly decreased ($P < 0.01$) expression in *Math5*^{-/-} mutants compared to WT controls by Student's *t*-test. (Scale bars, (F) 1,000 μ m, all others 100 μ m.)

Retinal Input Induces the Expression of FGF15. To investigate how retinal input regulates the recruitment of GABAergic interneurons into the visual thalamus, we assessed differential gene expression in the dLGN and vLGN in neonatal WT and *Math5*^{-/-} mutant mice (Fig. 3*A*) (29, 39). We focused our attention on genes that encode proteins capable of mediating intercellular communication, such as the extracellular matrix (ECM) proteins, morphogens, growth factors, and cell adhesion molecules. We identified one cue, FGF15, whose expression was reduced approximately fourfold in *Math5*^{-/-} mutant vLGN and dLGN (Fig. 3*B* and *C*). In fact, this was one of the only candidate genes identified that encodes a protein capable of mediating intercellular communication whose expression was significantly decreased in both the dLGN and vLGN of *Math5*^{-/-} mutants. A similar significant reduction in *Fgf15* mRNA expression was observed in RNA-sequencing (RNA-seq) analyses of *Math5*^{-/-} mutant dLGN (39).

FGFs are secreted cell signaling molecules that regulate proliferation, migration, differentiation, and synaptogenesis in the developing brain (43, 44). Unlike other FGFs, FGF15 has low affinity for heparin and, therefore, exhibits long-range actions (45). This is particularly important in the developing thalamus, where distinct nuclei are compartmentalized and segregated by specialized ECMs (rich in both chondroitin and heparin sulfate proteoglycans [CSPGs and HSPGs, respectively]) that bind traditional FGFs and limit their dispersion and range of action (29, 45–49). Thus, FGF15 exhibits unique features that make it an ideal candidate to recruit migrating thalamic and tectal GABAergic interneurons long distances into the developing visual thalamus (12, 13).

This led us to evaluate the developmental regulation of *Fgf15* mRNA expression in the dLGN and vLGN in previously generated RNA-seq datasets (38, 39). In both regions of the visual thalamus, *Fgf15* mRNA appeared highest at early postnatal ages (P3) and was largely absent by and after eye-opening (P12 to P25) (Fig. 3*D* and *E*). To confirm these data, we generated riboprobes against *Fgf15* and performed in situ hybridization (ISH). At P3, we observed *Fgf15* expression in the dLGN, vLGN, and other retinorecipient regions (e.g., the pretectum and superior colliculus [SC]), but *Fgf15* was absent from other regions of the hypothalamus, thalamus (including the IGL), and midbrain (Fig. 3*F* and *G*). Interestingly, *Fgf15* mRNA was present in the optic tract between the SC and visual thalamus, the second proposed migratory path of GABAergic interneurons of the dLGN (13) (Fig. 3*F*).

Expression of *Fgf15* in all retinorecipient regions was transient, so that by P8 (and at all subsequent ages), few *Fgf15*-expressing cells were observed in the dLGN or vLGN (Fig. 3*H*). Importantly, significantly reduced numbers of *Fgf15*⁺ cells were observed in the vLGN and dLGN of *Math5*^{-/-} mutants at P3 (Fig. 3*I* and *J*), revealing that *Fgf15* expression was regulated by retinal input.

FGF15 Is Required for the Recruitment of GABAergic Interneurons into the Visual Thalamus.

The ability of FGFs to influence cell migration, the expression of *Fgf15* along a potential migratory path of interneurons, and the regulation of *Fgf15* expression by retinal input led us to hypothesize that FGF15 may be necessary for the recruitment of GABAergic interneurons into the neonatal visual thalamus. To test this, we employed *Fgf15*^{-/-} mutant mice, which lack functional FGF15, by deleting the entire third exon of the gene, which encodes for half of the protein, including the FGFR- and heparin-binding motifs (50, 51). While a significant fraction of *Fgf15*^{-/-} mutant mice die embryonically, some survive into adulthood (50, 52). *Fgf15*^{-/-} mutants that survive are viable, and their size and activity during development appear indistinguishable from littermate controls. Importantly, despite *Fgf15* expression in the embryonic retina (53, 54), we observed no changes in retinal morphology or lamination in *Fgf15*^{-/-} mutants (Fig. 4*A* and *B*). To assess whether the loss of *Fgf15* impaired the generation or distribution of RGCs, we immunostained mutant and control retinas with an antibody against RNA-binding protein with multiple splicing (RBPMS), which specifically labels RGCs (55). We observed similar numbers of RGCs in *Fgf15*^{-/-} mutants and controls (9.7 ± 1.8 [SD] RBPMS⁺ RGCs/100 μm^2 in controls vs. 9.5 ± 0.1 [SD] RBPMS⁺ RGCs/100 μm^2 in *Fgf15*^{-/-} mutants; $n = 3$). Similarly, immunostaining with antibodies against VGluT2, a synaptic vesicle-associated protein present only in retinal terminals in the visual thalamus (36, 56), revealed no significant differences in the number or distribution retinogeniculate synapses in *Fgf15*^{-/-} mutants (Fig. 4*C–E*). The area of the dLGN was also not significantly different between age-matched mutants and controls (cross-sectional area of the dLGN in P14 control = $264,934.96 \mu\text{m}^2 \pm 23,851.17$ [SD] and in P14 *Fgf15*^{-/-} mutant = $256,895.80 \mu\text{m}^2 \pm 16,139.54$ [SD]; two-way ANOVA $F_{(1, 48)} = 12.76$, $P = 0.087$; $n = 3$). However, when we used riboprobes against *Gad1*, the gene encoding GAD67, to label GABAergic interneurons, we observed a significant reduction in *Gad1*-expressing interneurons in both the dLGN and vLGN in the absence of functional FGF15 (Fig. 5*A–C*). While the number of

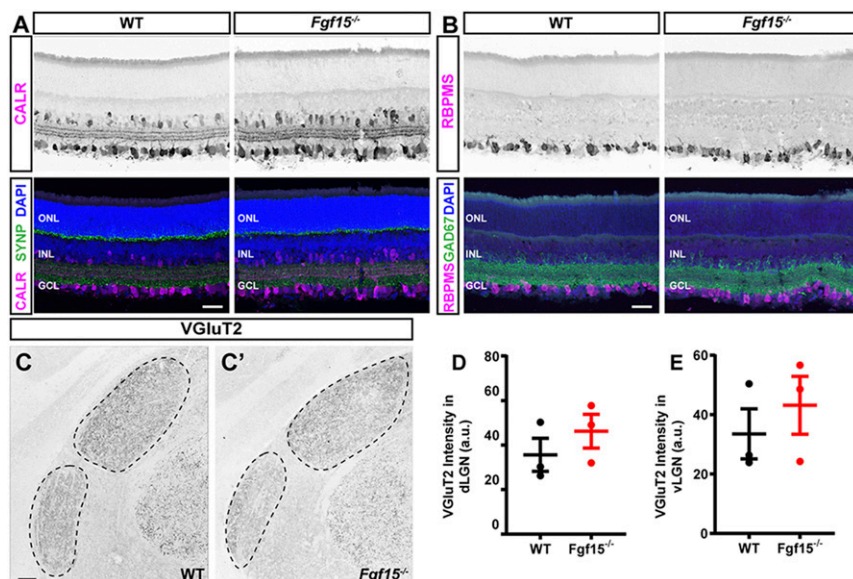


Fig. 4. Loss of functional FGF15 does not impair RGC development or central projections. (*A* and *B*) Immunolabeling of CALR/SYNP (*A*) or RBPMS/GAD67 (*B*) in *Fgf15*^{-/-} mutant and littermate control retinas. (Scale Bars, 50 μm .) (*C*) Immunolabeling for VGluT2 in P14 WT (*C*) and *Fgf15*^{-/-} mutant (*C'*) LGN. The vLGN and dLGN are outlined with dashed lines. (Scale Bars, 100 μm .) (*D* and *E*) Quantification of the average fluorescent intensity of immunolabeled VGluT2⁺ retinal terminals in the dLGN (*D*) and vLGN (*C*) in WT and *Fgf15*^{-/-} mutants. Data are shown as means \pm SEM; a.u., arbitrary units of average fluorescent intensity.

cells expressing *Gad1*⁺ was reduced in *Fgf15*^{-/-} mutants, we failed to detect changes in other cell types, such as the number or distribution of thalamocortical (TC) relay cells in the dLGN, which we labeled with riboprobes against the relay cell-specific gene *Lrrtm1* (38) (Fig. 5 D and E).

While mRNA analysis of *Gad1*⁺ interneurons appears to suggest that FGF15 is selectively necessary for interneuron migration into retino-recipient regions of the developing thalamus, these data could also be interpreted to suggest that FGF15 regulates *Gad1* mRNA expression by interneurons (12). To distinguish these possibilities, we crossed *Fgf15*^{-/-} mutants to the *Gad67*-GFP mice, in which high levels of GFP are generated at early ages even when *Gad1* mRNA levels remain low (33, 38). Analysis in *Gad67-GFP⁺::Fgf15*^{-/-} mice confirmed a reduction in GABAergic interneurons in both the dLGN and vLGN in the absence of functional FGF15 (Fig. 6 A and B). Reduced numbers of local inhibitory interneurons persisted in *Gad67-GFP⁺::Fgf15*^{-/-} mutants beyond eye-opening, suggesting that the reduced number of cells was not merely a delay in thalamic development in the absence of functional FGF15 (Fig. 6). Moreover, reduced numbers of GABAergic cells in the visual thalamus of *Fgf15*^{-/-} mutants did not appear to result from decreased neuronal proliferation or increased programmed cell death, based on *Otx2*- and *Casp3*-immunostaining,

respectively (SI Appendix, Fig. S4). Just as we observed increased numbers of GFP⁺ interneurons in inappropriate regions of the dorsal thalamus in *Gad67-GFP⁺::Math5*^{-/-} mutants (Fig. 2), significantly increased numbers of GFP⁺ cells were present in VB in the absence of functional FGF15 (Fig. 6).

Deficits in interneuron recruitment in *Gad67-GFP⁺::Fgf15*^{-/-} mice quantitatively phenocopy the decrease in GAD67-GFP⁺ cells in the visual thalamus and the increase in nonretino-recipient thalamic nuclei in *Gad67-GFP⁺::Math5*^{-/-} mice (Figs. 1, 5, and 6). However, we did not detect an alteration in interneuron spacing within the dLGN in *Fgf15*^{-/-} mutants (Fig. 6 A and B). Thus, while FGF15 is necessary for the recruitment of interneurons into dLGN, it appears that other retinal input-dependent mechanisms are required for the proper spacing of interneurons within this region of visual thalamus.

FGF15 Is Generated by Astrocytes in the Visual Thalamus. Since retinal input is required for FGF15 expression, we suspected that this FGF was generated by retino-recipient neurons in the dLGN and vLGN. To test this hypothesis, we performed ISH with *Fgf15* riboprobes in P3 *Crh-Cre::Rosa-Stop-tdT* reporter mice, in which a population of dLGN TC cells are fluorescently labeled (38). There was no coexpression of *Fgf15* in tdT⁺ TC neurons (Fig. 7A). Since only a fraction of TC neurons are labeled in these mice at this age (and none are labeled in the vLGN), we confirmed that neurons in the visual thalamus do not generate FGF15 by assessing coexpression of *Fgf15* mRNA with NeuN and Calbindin (CALB). *Fgf15* mRNA was not detected in any NeuN⁺ or CALB⁺ neurons in the visual thalamus (SI Appendix, Fig. S5). Since not all interneurons are labeled by NeuN-immunolabeling, and are significantly reduced in number in the visual thalamus of *Math5*^{-/-} mutants, we next assessed *Fgf15* mRNA expression in *Gad67*-GFP mice. We detected no colocalization of *Fgf15* mRNA with GFP⁺ interneurons (Fig. 7B). Finally, we tested whether glial cells generate FGF15 by performing ISH for *Fgf15* in *Aldh1l1-GFP* reporter mice, in which all thalamic astrocytes are labeled with GFP (57). These data revealed that not all GFP⁺ astrocytes generated *Fgf15*, but all *Fgf15*-expressing cells, were GFP⁺ astrocytes (Fig. 7C) (100% of *Fgf15*⁺ cells were GFP⁺ in both the dLGN and vLGN; 10.4 ± 2.3% [SD] of GFP⁺ astrocytes were *Fgf15*⁺ in the dLGN; 14.2 ± 3.2% [SD] of GFP⁺ astrocytes were *Fgf15*⁺ in the vLGN; n = 5). Similarly, *Fgf15*-expressing cells in the SC and the optic tract were *Aldh1l1-GFP*-labeled astrocytes (SI Appendix, Fig. S5). Taken together, these results suggest that retinal axons signal through astrocytes to induce the expression of FGF15 to influence GABAergic interneuron recruitment.

These unexpected results could be interpreted to suggest that either the number of astrocytes was reduced in *Math5*^{-/-} mutants (thus indirectly reducing the expression of *Fgf15* mRNA) or that astrocytic expression of *Fgf15* was dependent upon retinal input to the visual thalamus. To test whether there were reduced numbers of astrocytes in *Math5*^{-/-} mutants, we reexamined the expression of several astrocytic genes in the microarray dataset comparing the P2 WT and *Math5*^{-/-} mutant visual thalamus (29). No significant changes in the expression of astrocyte enriched genes (*Gfap*, *Aldh1l1*, *Slc1a2*, *S100b*, and *Aldoc*) (57) were observed in the *Math5*^{-/-} mutant thalamus (Fig. 8 A and B). Moreover, a normal distribution of astrocytes was observed in the visual thalamus of both *Math5*^{-/-} and *Fgf15*^{-/-} mutants (Fig. 8 C–N and SI Appendix, Fig. S6). Thus, changes in *Fgf15* expression in the absence of retinal input does not appear to be the result of altered astrocyte numbers in the denervated visual thalamus, and instead suggests retinal input induces the expression of *Fgf15* by astrocytes.

Discussion

A number of recent studies have revealed important roles for retinal input in patterning the cellular and molecular landscape of the developing visual thalamus (12, 25, 29, 30, 35, 39). Here, we add to this emergent knowledge by demonstrating that retinal

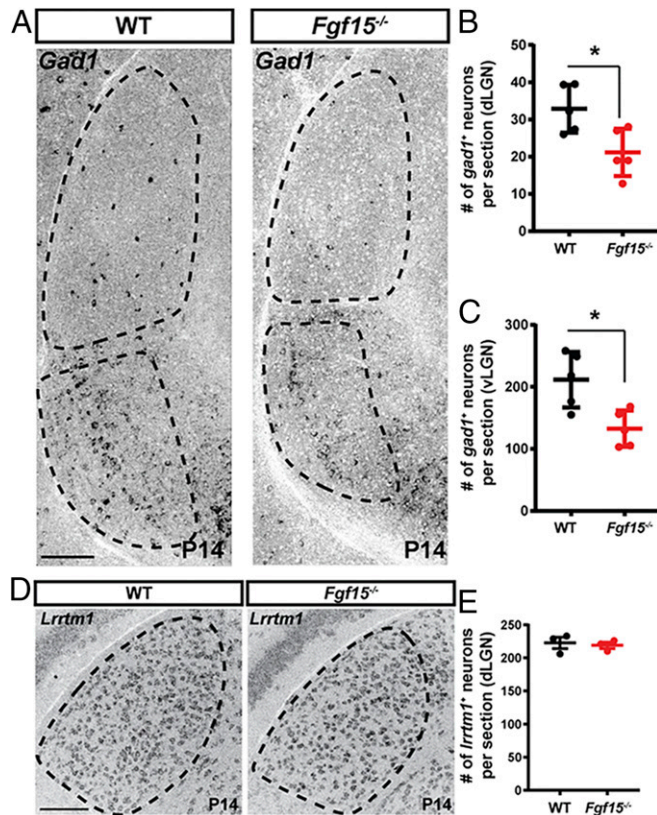


Fig. 5. Reduced numbers of *Gad1*⁺ cells in visual thalamus in the absence of functional FGF15. (A) ISH for *Gad1* mRNA revealed reduced numbers of *Gad1*⁺ cells in the dLGN and vLGN of P14 *Fgf15*^{-/-} mutants compared with littermate controls. (B and C) Quantification of *Gad1*⁺ cells in the dLGN (B) and vLGN (C) of P14 *Fgf15*^{-/-} mutants compared with littermate controls (WT). Bars represent means ± SEM. Asterisks (*) represent significantly decreased expression in *Math5*^{-/-} mutants compared to WT controls by Student's *t*-test (*P* < 0.01). (D) ISH for *Lrrtm1* mRNA revealed a normal distribution of relay cells in the dLGN and vLGN of P14 *Fgf15*^{-/-} mutants compared with littermate controls. (E) Quantification of *Lrrtm1*⁺ cells in dLGN of P14 *Fgf15*^{-/-} mutants compared with littermate controls (WT). Bars represent means ± SEM. (Scale bars, 100 μm for A and D.)

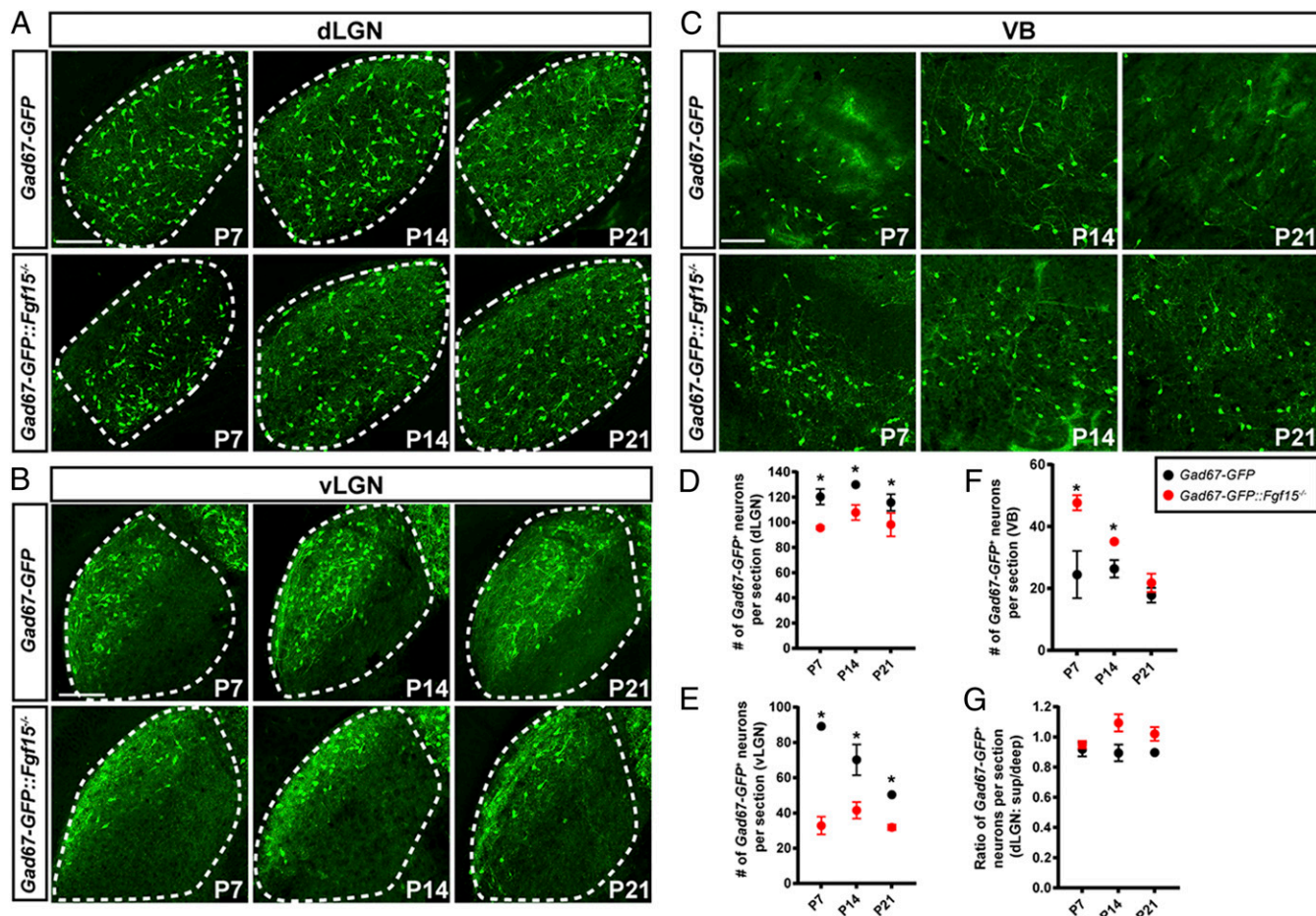


Fig. 6. FGF15 is required for *Gad67-GFP*⁺ interneuron recruitment into the visual thalamus. (A–C) Developmental distribution of GFP⁺ interneurons in dLGN (A), vLGN (B), and VB (C) of *Gad67-GFP* and *Gad67-GFP::Fgf15*^{-/-} mice. (Scale bars, 70 μ m.) (D–F) Quantification of the developmental distribution of GFP⁺ interneurons in the dLGN (D), vLGN (E), and VB (F) of *Gad67-GFP* and *Gad67-GFP::Fgf15*^{-/-} mice. Data represent means \pm SEM. Asterisks (*) represent significantly decreased interneuron number in *Fgf15*^{-/-};*Gad67-GFP* mutants compared to *Gad67-GFP* controls [in D, $F_{(1, 48)} = 38.8$, $P < 0.0001$; Holm–Sidak post hoc test, all $P < 0.006$; in E, $F_{(2, 72)} = 64.45$, $P < 0.0001$; Holm–Sidak post hoc test, all $P < 0.001$; in F, $F_{(1, 48)} = 19.97$, $P < 0.001$; P7, $P < 0.0001$; P14, $P = 0.033$]. (G) Quantification of interneuron distribution within dLGN of *Gad67-GFP* and *Gad67-GFP::Fgf15*^{-/-} mice as in Fig. 1E. Data points represent means \pm SEM. No statistical differences were observed between *Gad67-GFP::Fgf15*^{-/-} dLGN at different ages [$F_{(2, 48)} = 3.77$, $P = 0.301$; Holm–Sidak post hoc test, all $P > 0.552$] or between mutant and control dLGN [$F_{(1, 48)} = 3.998$, $P = 0.512$; Holm–Sidak post hoc test, all $P > 0.378$].

input regulates the recruitment of GABAergic interneurons into the dLGN and vLGN (Fig. 9). Since the arrival and arborization of retinal input precedes nonretinal aspects of visual thalamus development (including the arrival of both GABAergic interneurons and nonretinal inputs) (12, 29), we interpret these studies to suggest that molecular or activity-related signals from the retina influences their development. However, it is possible that the influence of retinal input is indirect. For example, the loss of retinal input accelerates both the loss of growth-inhibitory CSPGs from the dLGN (29) and the arrival of corticogeniculate axons (29). In the context of studies here, the early arrival of corticogeniculate axons could be outcompeting migrating GABAergic interneurons for real estate in the developing dLGN. While this possibility may seem attractive since GABAergic interneurons and prematurely invading cortical axons occupy nonoverlapping domains of the perinatal *Math5*^{-/-} mutant dLGN (29) (Fig. 1), it is unlikely to contribute to retinal input-dependent interneuron migration defects since these corticogeniculate axons do not enter or innervate the vLGN (58). However, results presented here suggest an alternative indirect pathway for retinal input to influence GABAergic interneuron migration into the visual thalamus. Specifically, retinal input induces the expression of FGF15 by thalamic astrocytes and the loss of functional FGF15 impairs interneuron recruitment into both the

dLGN and vLGN (Fig. 9). Thus, our data suggest that astrocytes, both those in the visual thalamus and those in the migratory path of GABAergic interneurons, direct the long-distance recruitment of GABAergic interneurons from thalamic and tectal progenitor zones (12, 13). This does not exclude the possibility that retinal axons also contribute to interneuron migration more directly. For example, RGCs could generate FGF15 and secrete it into the developing visual thalamus. While FGF15 is generated in the embryonic retina (53, 54), we found no evidence that RGCs generate this FGF during neonatal development (SI Appendix, Fig. S5). Of course, RGC axons could also express or secrete other motogenic cues that contribute to interneuron recruitment or spacing in the developing visual thalamus.

Thalamic Interneurons Migrate through Growth Inhibitory ECM Molecules. While the exact source of thalamic GABAergic progenitors and their migratory path are up for debate (12, 13), it is clear that these migratory neurons are capable of crossing boundaries between thalamic nuclei (in WT mice and both mutants studied here). What is surprising about this is that thalamic nuclei are compartmentalized by growth-inhibitory CSPGs (29, 46–49). For example, Aggrecan, a CSPG that repels axonal growth and embryonic neuronal migration (59, 60) is significantly enriched in

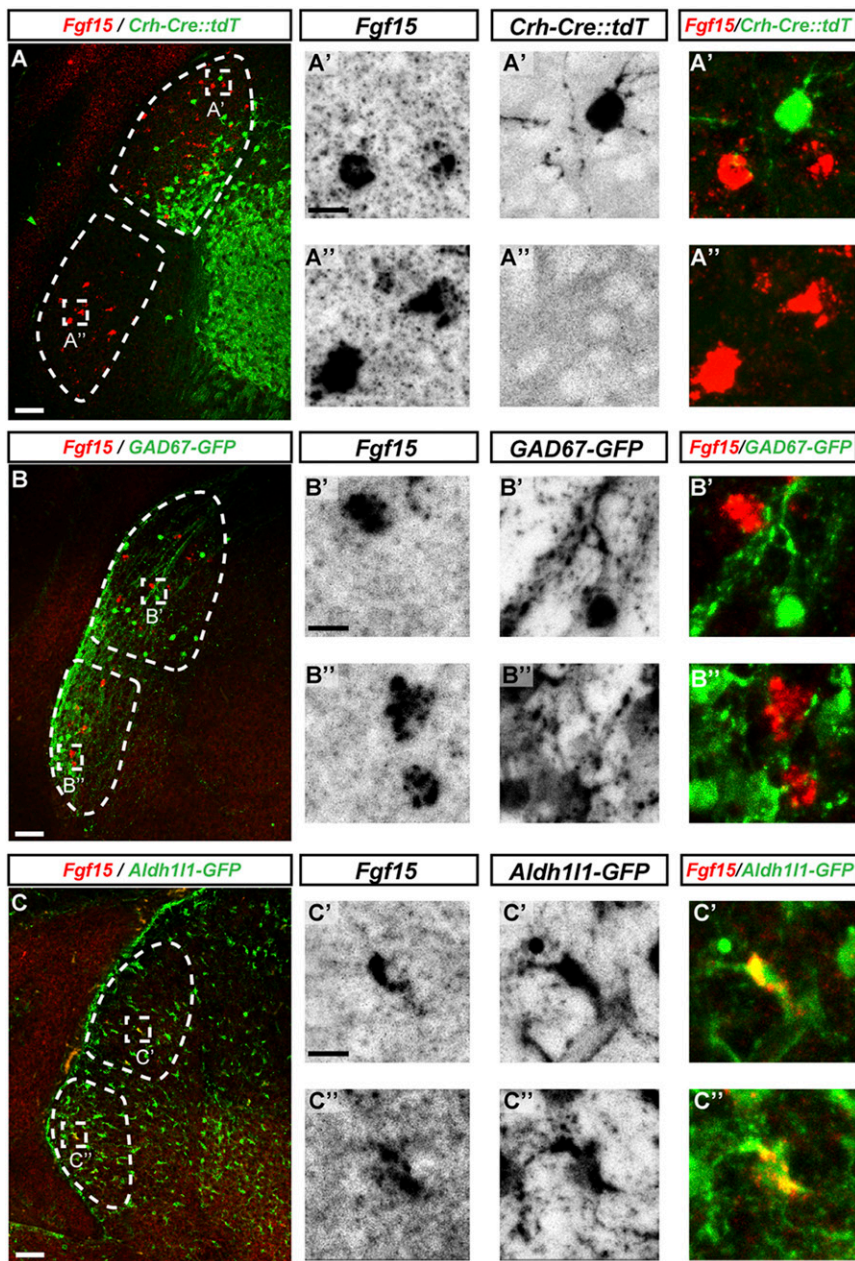


Fig. 7. Astrocytes express *Fgf15* in visual thalamus. (A) ISH *Fgf15* in the visual thalamus of P3 *Crh-Cre::tdT* transgenic mice revealed no expression by relay cells. (A') High-magnification image of *Fgf15*-expressing cells (red) and *Crh-Cre::tdT*⁺ relay cells (green) in the P3 dLGN. (A'') High-magnification image of *Fgf15*-expressing cells (red) in the vLGN. (B) ISH *Fgf15* in the visual thalamus of P3 *Gad67-GFP* mice revealed no expression by GABAergic interneurons. (B') High-magnification image of *Fgf15*-expressing cells (red) and interneurons (green) in the P3 dLGN. (B'') High-magnification image of *Fgf15*-expressing cells (red) and interneurons (green) in the P3 vLGN. (C) ISH *Fgf15* in the visual thalamus of P3 *Aldh11-GFP* mice revealed expression by astrocytes. (C') High-magnification image of *Fgf15*⁺/GFP⁺ astrocytes dLGN. (C'') High-magnification image of *Fgf15*⁺/GFP⁺ astrocytes vLGN. (Scale bars, 100 μm for A–C and 20 μm for A', A'', B', B'', C', and C'').

perinatal mouse dLGN compared to all other regions of the dorsal and ventral thalamus, including the vLGN (29). Data presented here demonstrate that GFP⁺ interneurons in *Gad67-GFP* mice are capable of migrating into both the dLGN and vLGN despite these significant differences in Aggrecan distribution. Similarly, misrouted GFP⁺ interneurons in *Gad67-GFP::Math5*^{-/-} and *Gad67-GFP::Fgf15*^{-/-} mutants appear equipped to migrate across thalamic boundaries and into inappropriate thalamic nuclei with distinct CSPG expression (46, 48, 49). At present, it is unclear how migrating thalamic GABAergic interneurons cross these CSPG-rich boundaries; however, neurotrophin or α3β1 integrin signaling are both sufficient to promote growth on inhibitory CSPGs in other brain regions (61, 62). Cortical interneurons labeled in these *Gad67-GFP* mice are known to express neurotrophin receptors and α3β1 integrin (33, 63–65); therefore, it is possible that migratory thalamic GABAergic neurons also express these receptors.

Astrocytes Influence Thalamic Interneuron Migration. While roles for astrocytes and radial glial cells in directing neuronal migration in the neocortex, cerebellum, and other brain regions are well-appreciated (3, 66, 67), they differ from the mechanisms identified here. For example, radial migration of excitatory neurons in the neocortex and cerebellum (and other brain regions) depends on glial-derived cell adhesion molecules (such as astrotactin, cadherins, neuregulin, and integrins) that promote contact-mediated adhesion between glial processes and migrating neurons (68–74). However, cortical GABAergic interneurons do not migrate along glial processes, and instead are guided tangentially by chemoattractive and chemorepulsive cues, such as semaphorins, slits, neurotrophins, and chemokines (72, 75–79). At present it remains unclear whether these chemoattractants or chemorepellents are released from astrocytes. However, we show here that astrocytes generate *Fgf15* in the developing thalamus and, like the chemoattractants described above, FGFs have well-established roles as chemoattractants inside and outside of the nervous system (43, 80,

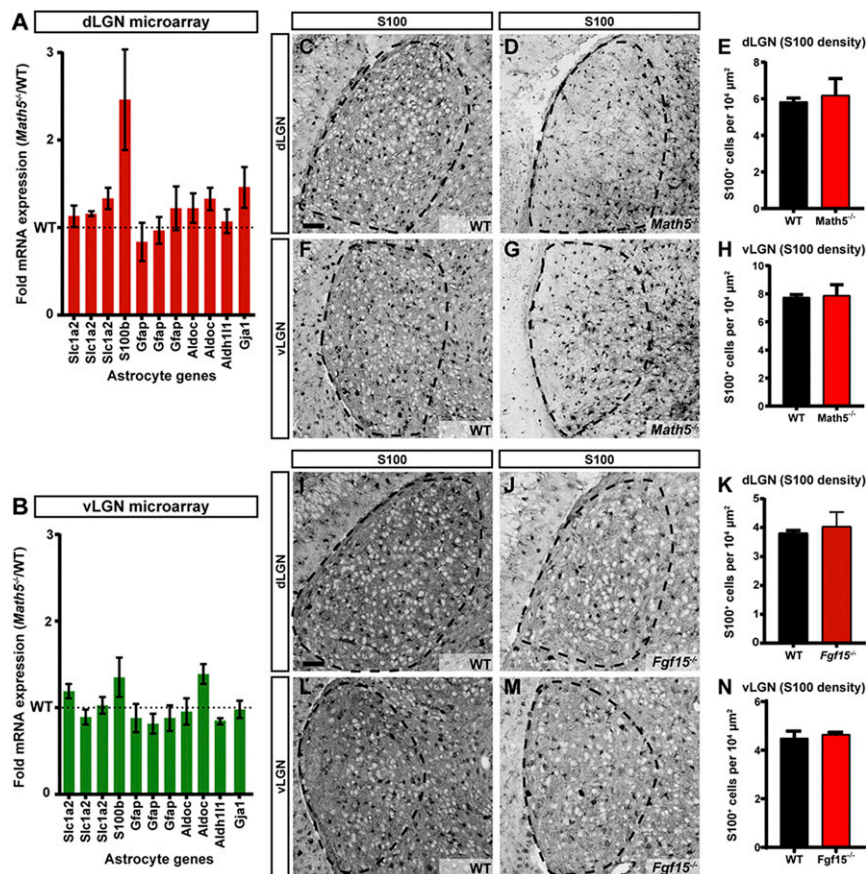


Fig. 8. Loss of retinal input or *Fgf15* does not impact the distribution of astrocytes in the visual thalamus. (A and B) Microarray dataset comparing the expression of several astrocytic markers between the P2 WT and *Math5*^{-/-} mutant visual thalamus (29). Dashed line represents expression levels in WT. Data are shown as means \pm SEM. (C and D) Immunostaining for the astrocytic marker S100 in the WT (C) and *Math5*^{-/-} (D) dLGN (outlined with dashed lines). (E) Quantification of S100⁺ cells in the dLGN of WT and *Math5*^{-/-} mice. Data are shown as means \pm SEM. (F and G) Immunostaining for S100 in WT (F) and *Math5*^{-/-} (G) vLGN (outlined with dashed lines). (H) Quantification of S100⁺ cells in the vLGN of WT and *Math5*^{-/-} mice. Data are shown as means \pm SEM. (I and J) Immunostaining for S100 in WT (I) and *Fgf15*^{-/-} (J) dLGN (outlined with dashed lines). (K) Quantification of S100⁺ cells in the dLGN of WT and *Fgf15*^{-/-} mice. Data are shown as means \pm SEM. (L and M) Immunostaining for S100 in WT (L) and *Fgf15*^{-/-} (M) vLGN (outlined with dashed lines). (N) Quantification of S100⁺ cells in the vLGN of WT and *Fgf15*^{-/-} mice. Data are shown as means \pm SEM. (Scale bars, 50 μ m for C–G; 70 μ m for I–M.)

81). FGFs, including FGF15, signal through FGFRs to regulate neural migration and circuit formation (43, 45, 82, 83). Importantly, GABAergic interneurons express a number of these FGFRs during early brain development (44, 84–86). Thus, results from the studies presented here suggest that astrocyte-derived FGFs may act as chemoattractants in the long-distance recruitment of GABAergic interneurons to the developing visual thalamus. As such, an important contribution of this work is that it is unique as a study implicating axonal innervation in regulating astrocytic expression of a potential chemoattractant cue.

An unresolved question is how retinal inputs signal to astrocytes to induce *Fgf15* expression. One possibility is that activity drives these events. Application of tetrodotoxin in thalamic slice cultures impairs the velocity of migrating interneurons within the dLGN (12). Indeed, neurotransmitters, such as the glutamate released by retinal axons, have been shown to contribute to neuronal migration in other brain regions (87–89). Whether neurotransmitters or neural activity alter FGF15 expression remains unclear. An alternative possibility is that *Fgf15* expression and interneuron migration are dependent upon other factors secreted by retinal axons, such as morphogens, growth factors, and ECM proteins. For example, retinal axons are known to release Sonic Hedgehog (SHH) (90, 91), a known inducer of FGF15 expression (92), and astrocytes express the canonical SHH receptors required to respond to gradients of SHH (90, 93, 94). Of

course, these possibilities are not mutually exclusive, and future efforts will be needed to tease apart the role of activity and axon-derived factors in these aspects of thalamic development.

While our results suggest that astrocyte-derived FGF15 is essential for the recruitment of GABAergic interneurons, the loss of functional FGF15 did not phenocopy all of the defects in thalamic interneuron recruitment associated with the loss of retinal input (12, 35). For example, the loss of functional FGF15 failed to influence interneuron spacing within these regions of the visual thalamus. This suggests that there are at least two mechanisms responsible for retinal input-dependent interneuron development in the visual thalamus, one that involves FGF15-dependent long-range migration of interneurons and another that controls interneuron dispersal within visual thalamic nuclei. In a similar fashion, distinct mechanisms contribute to GABAergic interneuron migration in the developing neocortex (3). For example, chemokine signaling is required for local, intracortical migration of interneurons but not for their long-range migration to the neocortex from germinal zones (76, 78, 79). Unfortunately, chemokine expression in the dLGN and vLGN did not appear to be regulated by retinal input (29, 39), so yet-to-be identified cues must regulate intrathalamic interneuron migration and spacing. Alternatively, cell adhesion molecules may contribute to interneuron spacing in the developing thalamus. In retina, the Down syndrome cell adhesion molecule (DSCAM) family of cell

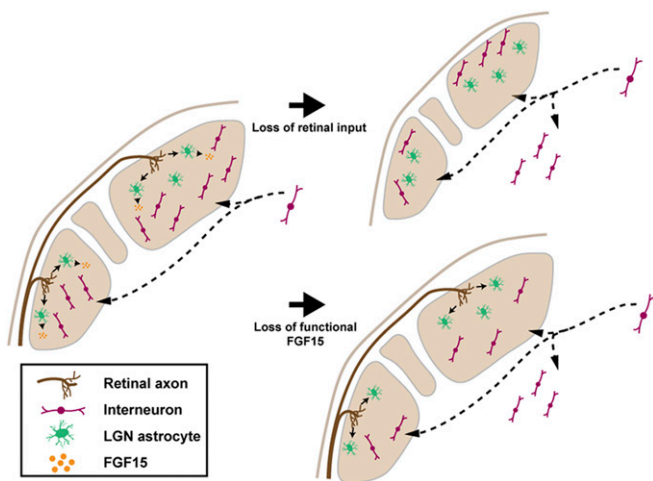


Fig. 9. Retinal inputs signal astrocytes to recruit interneurons into the visual thalamus. Schematic summarizing the role of retinal input and astrocyte-derived FGF15 in the recruitment of GABAergic neurons into the dLGN and vLGN.

adhesion molecules regulates spacing, but not laminar distribution, of retinal interneurons (and RGCs) (95). Our transcriptomic analyses indicate both *DSCAM* and *DSCAML1* are generated in the developing vLGN and dLGN (38), but their early postnatal expression in these regions seems to not depend on the presence of retinal inputs (29, 39). Future studies are needed to identify and characterize RGC- or target-derived candidates that regulate interneuron spacing in visual thalamus.

Astrocyte Diversity in the Visual Thalamus. On a final note, it is worth mentioning that only a fraction of astrocytes in the visual thalamus express *Fgf15*, even in the presence of retinal input. It is possible that such diversity merely represents asynchronous expression of this FGF by developing astrocytes. However, astrocytes in regions of the visual thalamus that lack GFP⁺ GABAergic interneurons in *Gad67-GFP* mice (such as the IGL) do not generate FGF15. Thus, we interpret these results to suggest a heterogeneity of thalamic astrocytes, not only between different regions of the visual thalamus but even within a single nucleus. With advances in single-cell transcriptomics, we are better defining such heterogeneity between neuronal subtypes in the developing or adult brain (for example, GABAergic cortical interneurons) (1, 96, 97). However, our understanding of astrocyte diversity in most brain regions remain limited. Moreover, our understanding of cellular heterogeneity in the vLGN and dLGN (at the transcriptome level) also remains limited (14, 98). Analysis of the data from one of these studies hints that at least two populations of transcriptionally distinct astrocytes do indeed exist in the developing dLGN (14). Of course, more traditional immunohistochemical approaches already support the notion of astrocyte heterogeneity in the visual thalamus; for example, astrocytes in the IGL differ significantly from those in the adjacent retinorecipient nuclei (58, 99). What defines these unique populations of thalamic astrocytes and what specific functions they exhibit in the thalamus remain to be identified.

Materials and Methods

Mouse Lines and Husbandry. C57/BL6 mice were obtained from Charles River or Harlan. *Gad67-GFP* mice (stock #007677) were obtained from the Jackson Laboratory. *Crh-Cre* mice (stock #030850-UCD) were obtained from the Mutant Mouse Resource and Research Center. *Math5^{-/-}* (stock #042298-UCD) (32), *Fgf15^{-/-}* (stock #032840-UCD) (50), and *Aldh111-EGFP* (stock #011015-UCD) mice were obtained from S. W. Wang, University of Texas MD Anderson Cancer Center, Houston, TX, S. Kliewer, University of Texas Southwestern Medical Center, Dallas, TX, and S. Robel, Virginia

Tech, Roanoke, VA, respectively. Mice of both genders have been used in this study. Mice were housed in a 12-h dark/light cycle and had ad libitum access to food and water. All experiments were performed in compliance with National Institutes of Health guidelines and protocols and were approved by the Virginia Polytechnic Institute and State University and the University of Louisville Institutional Animal Care and Use Committee.

Tissue Preparation and Immunohistochemistry. Deeply anesthetized mice were transcardially perfused with PBS (pH 7.4) and 4% paraformaldehyde in PBS (PFA; pH 7.4). Brains were excised and postfixed overnight in 4% PFA, then transferred to PBS. Using a vibratome (Leica VT1200S), thalamic sections (70 μ m) were cut in the coronal plane. Sections including the vLGN, dLGN, lateral posterior nucleus, and VB were collected, mounted with Prolong Gold (Invitrogen), and cover-slipped for confocal microscopy. For immunohistochemistry, tissues were cryopreserved in 30% sucrose solution for 2 to 3 d, embedded in Tissue Freezing Medium (Electron Microscopy Sciences), and cryosectioned (16- μ m sections). Slides were incubated in blocking buffer (2.5% BSA, 5% normal goat serum, 0.1% Triton-X in PBS) for 1 h. Tissues were stained using primary antibodies (CASP3, 1:400 [cat #9661-5, Cell Signaling], 1:800 [cat #9664-5, Cell Signaling]; GFP, 1:250 [cat #A-11122, Life Technologies]; Calb, 1:5,000 [cat #CB-38a, Swant]; NeuN, 1:250 [cat #MAB377, Millipore]; S100 β , 1:200 [cat #Z0311, Agilent Dako]; calretinin [CALR], 1:2,000 [cat #AB5054, Millipore]; RBPM5, 1:500 [cat #1830-RBPM5, Phosphosolutions]; GAD67, 1:1,000 [cat #MAB5406, Millipore]; synaptophysin (SYNP), 1:500 [cat #101 011, Synaptic Systems]; and OTX2, 1:200 [cat #MA5-15854, Thermo Fisher Scientific]) for >12 h at 4 $^{\circ}$ C followed by fluorescently conjugated secondary antibodies (1:1,000 in blocking buffer) for 1 h at room temperature. Finally, slides were mounted with Prolong Gold and cover-slipped for confocal microscopy. Images were acquired on either a Zeiss LSM 700 or an Olympus FV1200BX61 confocal microscope. When comparing sections from different age groups or genotypes, images were acquired with identical parameters. A minimum of three animals (per genotype and per age) were compared in all immunohistochemistry experiments.

Riboprobe Production. pCMV-SPORT6 Plasmids carrying *Fgf15* (cat #5066286) and *Lrrtm1* (cat #5321979) were obtained from GE Dharmacon. *Gad1* 1Kb cDNA (corresponding to nucleotides 1099 to 2081), *Asic4* 1.1Kb cDNA (corresponding to nucleotides 1173 to 2320), and *Gja1* 1.1Kb cDNA (corresponding to nucleotides 714 to 1854) was generated using SuperScript II Reverse Transcriptase First Strand cDNA Synthesis kit (cat #18064014, Invitrogen) according to the manufacturer's manual, amplified by PCR using primers mentioned in the primers list, gel purified, and then cloned into a pGEM-T Easy Vector using pGEM-T Easy Vector kit, (cat #A1360, Promega) according to the kit manual. Sense and antisense riboprobes against *Fgf15*, *Lrrtm1*, *Gja1*, and *Gad1* were synthesized from 5- μ g linearized plasmids using digoxigenin-(DIG) or fluorescein-labeled uridylyltransferase (UTP) (cat #11685619910, cat #11277073910, Roche) and the MAXscript in vitro Transcription Kit (cat #AM1312, Ambion) according to the kit manual. Five micrograms of Riboprobes (20 μ L) were hydrolyzed into ~0.5-kb fragments by adding 80 μ L of water, 4 μ L of NaHCO₃ (1 M), 6 μ L Na₂CO₃ (1 M) and incubating the mixture in 60 $^{\circ}$ C for specific amounts of time determined for each probe by the following formula: Time = $(X_{kb} - 0.5)/(X_{kb} \times 0.055)$, where X is the full length of the RNA probe. RNA fragments were finally precipitated in 250 μ L 100% ethanol containing 5 μ L acetic acid, 10 μ L NaCl (5 M), and 1 μ L glycogen (5 mg/mL). Finally, the riboprobes dissolved in 50 μ L of RNase-free water.

In Situ Hybridization. ISH was performed on 16- μ m sections prepared as described previously (63, 100). Slides were air dried for 30 min at room temperature and washed with PBS for 5 min to remove OTC. Sections were fixed in 4% PFA for 10 min, washed with PBS for 15 min, incubated in proteinase K solution (1 μ g/mL in 50 mM Tris PH 7.5, 5 mM EDTA) for 10 min, washed with PBS for 5 min, incubated in 4% PFA for 5 min, washed with PBS for 15 min, incubated in acetylation solution (196.6 mL water, 2.6 mL triethanolamin, 0.35 mL HCl, 0.5 mL acetic acid) for 10 min, washed with PBS for 10 min, incubated in 0.1% triton (in PBS) for 30 min, washed with PBS for 40 min, incubated in 0.3% H₂O₂ (in water) for 30 min, washed with PBS for 10 min, prehybridized with hybridization solution (50 mL of Sigma 2 \times prehyb solution, 25 mg Roche yeast RNA, and 8 mg heparin) for 1 h, hybridized with 50 μ L of heat-denatured diluted riboprobes (1 to 2 μ L of riboprobe in 50 μ L hybridization solution heated for 10 min in 70 $^{\circ}$ C), mounted with coverslips and kept at 60 $^{\circ}$ C overnight. On day 2, coverslips were gently removed in 60 $^{\circ}$ C preheated 2 \times saline-sodium citrate (SSC) buffer, and slides were washed five times in 60 $^{\circ}$ C preheated 0.2 \times SSC buffer for 2 to 3 h at 60 $^{\circ}$ C. Slides were washed three times with Tris-buffered saline (TBS) and blocked for 1 h with blocking

buffer (0.2% Roche blocking reagent, 10% lamb serum in TBS) prior to overnight 4 °C incubation with horseradish peroxidase (POD)-conjugated anti-DIG or antifluorescent antibodies (cat #11426346910 and cat #11207733910, Roche). On day 3, bound riboprobes were detected by staining with Tyramide Signal Amplification (TSA) system (cat #NEL75300 1KT, PerkinElmer). A minimum of three animals (per genotype and per age) were used in all ISH comparison experiments.

Quantification of the Number and Distribution of Interneurons. To quantify the number of interneurons within each region, z-stacked datasets were uploaded into Imaris software (Bitplane, v8.4.1) and ImageJ (v1.50h, NIH). DAPI was used to delineate the borders of thalamic nuclei. Cell counts were obtained from three sections within the middle of each region. Final values were the average of cell counts from at least three mice. To determine the distribution of interneurons in the dLGN, we divided the dLGN into “top” and “bottom” sections. Three straight lines (Straight, Segmented tool) were drawn across the width of the dLGN: The bottom border, the widest point, and the top. The midpoints of each line were then connected. The total number of interneurons in each sector was calculated and used to generate a top-to-bottom tier ratio. A *t*-test or two-way ANOVA analysis (Prism 7.0) was used to determine any significant change in the number and distribution of interneurons between groups. The post hoc Holm–Sidak test was

applied twice to allow for multiple comparisons within and between group across postnatal weeks. To compare the ratios of cells between the dLGN and other thalamic nuclei χ^2 analysis was performed.

Quantification of the Density and Intensity of Staining. Intensity and density of the signals in immunostained images of the dLGN, vLGN, and visual cortex were measured in ImageJ. Three to seven animals (three sections per animal) were analyzed per genotype and age and the mean values were compared between groups. A *t*-test or ANOVA was used to determine any significant difference of the mean values between groups.

Data Availability. Microarray and RNA-seq experiments on the developing visual thalamus in WT and *Math5*^{-/-} have been made publicly available and are described in refs. 29, 38, and 39. All other data presented here are included in the main text and *SI Appendix*.

ACKNOWLEDGMENTS. We thank Drs. S. Robel, S. Kliewer, and S. W. Wang for generously supplying *Aldh111-GFP*, *Fgf15*^{-/-}, and *Math5*^{-/-} mice, respectively; and Barbara O’Steen for her expert technical support. This work was supported by the National Institutes of Health Grants EY021222 (to M.A.F.), EY030568 (to M.A.F.), EY012716 (to W.G.), and NS113459 (to U.S.).

1. L. Lim *et al.*, Optimization of interneuron function by direct coupling of cell migration and axonal targeting. *Nat. Neurosci.* **21**, 920–931 (2018).
2. B. Wamsley, G. Fishell, Genetic and activity-dependent mechanisms underlying interneuron diversity. *Nat. Rev. Neurosci.* **18**, 299–309 (2017).
3. O. Marin, M. Valiente, X. Ge, L.-H. Tsai, Guiding neuronal cell migrations. *Cold Spring Harb. Perspect. Biol.* **2**, a001834 (2010).
4. W. Guido, Development, form, and function of the mouse visual thalamus. *J. Neurophysiol.* **120**, 211–225 (2018).
5. A. Monavafshani, U. Sabbagh, M. A. Fox, Not a one-trick pony: Diverse connectivity and functions of the rodent lateral geniculate complex. *Vis. Neurosci.* **34**, E012 (2017).
6. M. E. Harrington, The ventral lateral geniculate nucleus and the intergeniculate leaflet: Interrelated structures in the visual and circadian systems. *Neurosci. Biobehav. Rev.* **21**, 705–727 (1997).
7. R. Y. Moore, J. P. Card, Intergeniculate leaflet: An anatomically and functionally distinct subdivision of the lateral geniculate complex. *J. Comp. Neurol.* **344**, 403–430 (1994).
8. P. Arcelli, C. Frassoni, M. C. Regondi, S. De Biasi, R. Spreafico, GABAergic neurons in mammalian thalamus: A marker of thalamic complexity? *Brain Res. Bull.* **42**, 27–37 (1997).
9. L. Jaubert-Miazza *et al.*, Structural and functional composition of the developing retinogeniculate pathway in the mouse. *Vis. Neurosci.* **22**, 661–676 (2005).
10. M. Evangelio, M. García-Amado, F. Clascá, Thalamic projection neuron and interneuron numbers in the visual thalamic nuclei of the adult C57BL/6 mouse. *Front. Neuroanat.* **12**, 27 (2018).
11. M. Leist *et al.*, Two types of interneurons in the mouse lateral geniculate nucleus are characterized by different h-current density. *Sci. Rep.* **6**, 24904 (2016).
12. B. Golding *et al.*, Retinal input directs the recruitment of inhibitory interneurons into thalamic visual circuits. *Neuron* **81**, 1057–1069 (2014).
13. P. Jager *et al.*, Tectal-derived interneurons contribute to phasic and tonic inhibition in the visual thalamus. *Nat. Commun.* **7**, 13579 (2016).
14. B. T. Kalish *et al.*, Single-cell transcriptomics of the developing lateral geniculate nucleus reveals insights into circuit assembly and refinement. *Proc. Natl. Acad. Sci. U.S.A.* **115**, E1051–E1060 (2018).
15. R. W. Guillery, S. M. Sherman, Thalamic relay functions and their role in corticocortical communication: Generalizations from the visual system. *Neuron* **33**, 163–175 (2002).
16. T. A. Seabrook, R. N. El-Danaf, T. E. Krahe, M. A. Fox, W. Guido, Retinal input regulates the timing of corticogeniculate innervation. *J. Neurosci.* **33**, 10085–10097 (2013).
17. J. A. Hirsch, X. Wang, F. T. Sommer, L. M. Martinez, How inhibitory circuits in the thalamus serve vision. *Annu. Rev. Neurosci.* **38**, 309–329 (2015).
18. T. T. Norton, D. W. Godwin, Inhibitory GABAergic control of visual signals at the lateral geniculate nucleus. *Prog. Brain Res.* **90**, 193–217 (1992).
19. S. M. Sherman, Interneurons and triadic circuitry of the thalamus. *Trends Neurosci.* **27**, 670–675 (2004).
20. D. M. Blitz, W. G. Regehr, Timing and specificity of feed-forward inhibition within the LGN. *Neuron* **45**, 917–928 (2005).
21. P. L. Gabbott, S. J. Bacon, Two types of interneuron in the dorsal lateral geniculate nucleus of the rat: A combined NADPH diaphorase histochemical and GABA immunocytochemical study. *J. Comp. Neurol.* **350**, 281–301 (1994).
22. N. Inamura, K. Ono, H. Takebayashi, B. Zalc, K. Ikenaka, Olig2 lineage cells generate GABAergic neurons in the prethalamic nuclei, including the zona incerta, ventral lateral geniculate nucleus and reticular thalamic nucleus. *Dev. Neurosci.* **33**, 118–129 (2011).
23. R. Y. Moore, J. C. Speh, GABA is the principal neurotransmitter of the circadian system. *Neurosci. Lett.* **150**, 112–116 (1993).
24. K. Yuge *et al.*, Region-specific gene expression in early postnatal mouse thalamus. *J. Comp. Neurol.* **519**, 544–561 (2011).
25. U. Sabbagh *et al.*, Distribution and development of molecularly distinct perineuronal nets in visual thalamus. *J. Neurochem.* **147**, 626–646 (2018).
26. M. E. Bickford *et al.*, Synaptic development of the mouse dorsal lateral geniculate nucleus. *J. Comp. Neurol.* **518**, 622–635 (2010).
27. G. Sokhadze, T. A. Seabrook, W. Guido, The absence of retinal input disrupts the development of cholinergic brainstem projections in the mouse dorsal lateral geniculate nucleus. *Neural Dev.* **13**, 27 (2018).
28. T. A. Seabrook, T. E. Krahe, G. Govindaiah, W. Guido, Interneurons in the mouse visual thalamus maintain a high degree of retinal convergence throughout postnatal development. *Neural Dev.* **8**, 24 (2013).
29. J. M. Brooks *et al.*, A molecular mechanism regulating the timing of corticogeniculate innervation. *Cell Rep.* **5**, 573–581 (2013).
30. E. Grant, A. Hoerder-Suabedissen, Z. Molnár, The regulation of corticofugal fiber targeting by retinal inputs. *Cereb. Cortex* **26**, 1336–1348 (2016).
31. N. L. Brown *et al.*, Math5 encodes a murine basic helix-loop-helix transcription factor expressed during early stages of retinal neurogenesis. *Development* **125**, 4821–4833 (1998).
32. S. W. Wang *et al.*, Requirement for math5 in the development of retinal ganglion cells. *Genes Dev.* **15**, 24–29 (2001).
33. B. Chattopadhyaya *et al.*, Experience and activity-dependent maturation of perisomatic GABAergic innervation in primary visual cortex during a postnatal critical period. *J. Neurosci.* **24**, 9598–9611 (2004).
34. T. Munsch, Y. Yanagawa, K. Obata, H. C. Pape, Dopaminergic control of local interneuron activity in the thalamus. *Eur. J. Neurosci.* **21**, 290–294 (2005).
35. N. E. Charalambakis, G. Govindaiah, P. W. Campbell, W. Guido, Developmental remodeling of thalamic interneurons requires retinal signaling. *J. Neurosci.* **39**, 3856–3866 (2019).
36. S. Hammer *et al.*, Nuclei-specific differences in nerve terminal distribution, morphology, and development in mouse visual thalamus. *Neural Dev.* **9**, 16 (2014).
37. R. N. El-Danaf *et al.*, Developmental remodeling of relay cells in the dorsal lateral geniculate nucleus in the absence of retinal input. *Neural Dev.* **10**, 19 (2015).
38. A. Monavafshani *et al.*, LRRTM1 underlies synaptic convergence in visual thalamus. *elife* **7**, e33498 (2018).
39. J. He *et al.*, Retinal-input-induced epigenetic dynamics in the developing mouse dorsal lateral geniculate nucleus. *Epigenetics Chromatin* **12**, 13 (2019).
40. D. R. McIlwain, T. Berger, T. W. Mak, Caspase functions in cell death and disease. *Cold Spring Harb. Perspect. Biol.* **5**, a008656 (2013).
41. R. M. Harris, A. E. Hendrickson, Local circuit neurons in the rat ventrobasal thalamus—A GABA immunocytochemical study. *Neuroscience* **21**, 229–236 (1987).
42. R. Spreafico, C. Frassoni, P. Arcelli, S. De Biasi, GABAergic interneurons in the somatosensory thalamus of the guinea-pig: A light and ultrastructural immunocytochemical investigation. *Neuroscience* **59**, 961–973 (1994).
43. I. Mason, Initiation to end point: The multiple roles of fibroblast growth factors in neural development. *Nat. Rev. Neurosci.* **8**, 583–596 (2007).
44. A. Terauchi *et al.*, Distinct FGFs promote differentiation of excitatory and inhibitory synapses. *Nature* **465**, 783–787 (2010).
45. D. M. Ornitz, N. Itoh, The fibroblast growth factor signaling pathway. *Wiley Interdiscip. Rev. Dev. Biol.* **4**, 215–266 (2015).
46. S. Hockfield, R. McKay, S. Hendry, E. Jones, A surface antigen that identifies ocular dominance columns in the visual cortex and laminar features of the lateral geniculate nucleus. *Cold Spring Harb. Symp. Quant. Biol.* **48**, 877–889 (1983).
47. M. Sahin, S. A. Slaugenhaupt, J. F. Gusella, S. Hockfield, Expression of PTPH1, a rat protein tyrosine phosphatase, is restricted to the derivatives of a specific diencephalic segment. *Proc. Natl. Acad. Sci. U.S.A.* **92**, 7859–7863 (1995).
48. J. W. Crabtree, P. C. Kind, Monoclonal antibody Cat-301 selectively identifies a subset of nuclei in the cat’s somatosensory thalamus. *J. Neurocytol.* **22**, 903–912 (1993).
49. T. M. Preuss, D. Gray, C. G. Cusick, Subdivisions of the motor and somatosensory thalamus of primates revealed with Wisteria floribunda agglutinin histochemistry. *Somatosens. Mot. Res.* **15**, 211–219 (1998).

50. T. J. Wright *et al.*, Mouse FGF15 is the ortholog of human and chick FGF19, but is not uniquely required for otic induction. *Dev. Biol.* **269**, 264–275 (2004).
51. J. D. Schumacher *et al.*, Direct and indirect effects of fibroblast growth factor (FGF) 15 and FGF19 on liver fibrosis development. *Hepatology*, 10.1002/hep.30810 (2019).
52. J. W. Vincentz, J. R. McWhirter, C. Murre, A. Baldini, Y. Furuta, Fgf15 is required for proper morphogenesis of the mouse cardiac outflow tract. *Genesis* **41**, 192–201 (2005).
53. H. Kurose *et al.*, Expression of Fibroblast growth factor 19 (Fgf19) during chicken embryogenesis and eye development, compared with Fgf15 expression in the mouse. *Gene Expr. Patterns* **4**, 687–693 (2004).
54. Y. Nakayama *et al.*, Fgf19 is required for zebrafish lens and retina development. *Dev. Biol.* **313**, 752–766 (2008).
55. A. R. Rodriguez, L. P. de Sevilla Müller, N. C. Brecha, The RNA binding protein RBPM5 is a selective marker of ganglion cells in the mammalian retina. *J. Comp. Neurol.* **522**, 1411–1443 (2014).
56. P. W. Land, E. Kyonka, L. Shamalla-Hannah, Vesicular glutamate transporters in the lateral geniculate nucleus: Expression of VGLUT2 by retinal terminals. *Brain Res.* **996**, 251–254 (2004).
57. J. D. Cahoy *et al.*, A transcriptome database for astrocytes, neurons, and oligodendrocytes: A new resource for understanding brain development and function. *J. Neurosci.* **28**, 264–278 (2008).
58. J. Su *et al.*, Reelin is required for class-specific retinogeniculate targeting. *J. Neurosci.* **31**, 575–586 (2011).
59. D. M. Snow, V. Lemmon, D. A. Carrino, A. I. Caplan, J. Silver, Sulfated proteoglycans in astroglial barriers inhibit neurite outgrowth in vitro. *Exp. Neurol.* **109**, 111–130 (1990).
60. M. L. Condic, D. M. Snow, P. C. Letourneau, Embryonic neurons adapt to the inhibitory proteoglycan aggrecan by increasing integrin expression. *J. Neurosci.* **19**, 10036–10043 (1999).
61. C. L. Tan *et al.*, Integrin activation promotes axon growth on inhibitory chondroitin sulfate proteoglycans by enhancing integrin signaling. *J. Neurosci.* **31**, 6289–6295 (2011).
62. F. Q. Zhou *et al.*, Neurotrophins support regenerative axon assembly over CSPGs by an ECM-integrin-independent mechanism. *J. Cell Sci.* **119**, 2787–2796 (2006).
63. J. Su *et al.*, Collagen-derived matricryptins promote inhibitory nerve terminal formation in the developing neocortex. *J. Cell Biol.* **212**, 721–736 (2016).
64. S. Patz, J. Grabert, T. Gorba, M. J. Wirth, P. Wahle, Parvalbumin expression in visual cortical interneurons depends on neuronal activity and TrkB ligands during an Early period of postnatal development. *Cereb. Cortex* **14**, 342–351 (2004).
65. Z. J. Huang *et al.*, BDNF regulates the maturation of inhibition and the critical period of plasticity in mouse visual cortex. *Cell* **98**, 739–755 (1999).
66. P. Rakic, R. S. Cameron, H. Komuro, Recognition, adhesion, transmembrane signaling and cell motility in guided neuronal migration. *Curr. Opin. Neurobiol.* **4**, 63–69 (1994).
67. M. E. Hatten, C. A. Mason, Mechanisms of glial-guided neuronal migration in vitro and in vivo. *Experientia* **46**, 907–916 (1990).
68. J. C. Edmondson, R. K. Liem, J. E. Kuster, M. E. Hatten, Astrotactin: A novel neuronal cell surface antigen that mediates neuron-astroglial interactions in cerebellar microcultures. *J. Cell Biol.* **106**, 505–517 (1988).
69. G. Fishell, M. E. Hatten, Astrotactin provides a receptor system for CNS neuronal migration. *Development* **113**, 755–765 (1991).
70. E. S. Anton, M. A. Marchionni, K. F. Lee, P. Rakic, Role of GGF/neuregulin signaling in interactions between migrating neurons and radial glia in the developing cerebral cortex. *Development* **124**, 3501–3510 (1997).
71. C. Rio, H. I. Rieff, P. Qi, T. S. Khurana, G. Corfas, Neuregulin and erbB receptors play a critical role in neuronal migration. *Neuron* **19**, 39–50 (1997).
72. O. Marin, J. L. Rubenstein, Cell migration in the forebrain. *Annu. Rev. Neurosci.* **26**, 441–483 (2003).
73. R. Belvindrah, D. Graus-Porta, S. Goebbels, K.-A. Nave, U. Müller, β 1 integrins in radial glia but not in migrating neurons are essential for the formation of cell layers in the cerebral cortex. *J. Neurosci.* **27**, 13854–13865 (2007).
74. Z. Horn, H. Behesti, M. E. Hatten, N-cadherin provides a *cis* and *trans* ligand for astrotactin that functions in glial-guided neuronal migration. *Proc. Natl. Acad. Sci. U.S.A.* **115**, 10556–10563 (2018).
75. W. Andrews *et al.*, The role of Slit-Robo signaling in the generation, migration and morphological differentiation of cortical interneurons. *Dev. Biol.* **313**, 648–658 (2008).
76. G. Li *et al.*, Regional distribution of cortical interneurons and development of inhibitory tone are regulated by Cxcl12/Cxcr4 signaling. *J. Neurosci.* **28**, 1085–1098 (2008).
77. O. Marin, J. L. Rubenstein, A long, remarkable journey: Tangential migration in the telencephalon. *Nat. Rev. Neurosci.* **2**, 780–790 (2001).
78. G. López-Bendito *et al.*, Chemokine signaling controls intracortical migration and final distribution of GABAergic interneurons. *J. Neurosci.* **28**, 1613–1624 (2008).
79. M.-C. Tiveron *et al.*, Molecular interaction between projection neuron precursors and invading interneurons via stromal-derived factor 1 (CXCL12)/CXCR4 signaling in the cortical subventricular zone/intermediate zone. *J. Neurosci.* **26**, 13273–13278 (2006).
80. Y. K. Bae, N. Trisnadi, S. Kadam, A. Stathopoulos, The role of FGF signaling in guiding coordinate movement of cell groups: Guidance cue and cell adhesion regulator? *Cell Adhes. Migr.* **6**, 397–403 (2012).
81. M. A. Brea, D. Wilson, D. G. Wilkinson, Q. Xu, Chemokine and Fgf signalling act as opposing guidance cues in formation of the lateral line primordium. *Development* **139**, 2246–2253 (2012).
82. H. Umemori, M. W. Linhoff, D. M. Ornitz, J. R. Sanes, FGF22 and its close relatives are presynaptic organizing molecules in the mammalian brain. *Cell* **118**, 257–270 (2004).
83. M. A. Fox *et al.*, Distinct target-derived signals organize formation, maturation, and maintenance of motor nerve terminals. *Cell* **129**, 179–193 (2007).
84. A. Dabrowski, A. Terauchi, C. Strong, H. Umemori, Distinct sets of FGF receptors sculpt excitatory and inhibitory synaptogenesis. *Development* **142**, 1818–1830 (2015).
85. G. Gutin *et al.*, FGF signalling generates ventral telencephalic cells independently of SHH. *Development* **133**, 2937–2946 (2006).
86. A. Miyake *et al.*, Fgf16 is required for specification of GABAergic neurons and oligodendrocytes in the zebrafish forebrain. *PLoS One* **9**, e110836 (2014).
87. J.-B. Manent *et al.*, A noncanonical release of GABA and glutamate modulates neuronal migration. *J. Neurosci.* **25**, 4755–4765 (2005).
88. J.-B. Manent, I. Jorquera, Y. Ben-Ari, L. Aniksztejn, A. Represa, Glutamate acting on AMPA but not NMDA receptors modulates the migration of hippocampal interneurons. *J. Neurosci.* **26**, 5901–5909 (2006).
89. H. J. Luhmann, A. Fukuda, W. Kilb, Control of cortical neuronal migration by glutamate and GABA. *Front. Cell. Neurosci.* **9**, 4 (2015).
90. V. A. Wallace, M. C. Raff, A role for Sonic hedgehog in axon-to-astrocyte signalling in the rodent optic nerve. *Development* **126**, 2901–2909 (1999).
91. J. Peng *et al.*, Sonic hedgehog is a remotely produced cue that controls axon guidance trans-axonally at a midline choice point. *Neuron* **97**, 326–340.e4 (2018).
92. H. Saitsu *et al.*, Expression of the mouse Fgf15 gene is directly initiated by Sonic hedgehog signaling in the diencephalon and midbrain. *Dev. Dyn.* **232**, 282–292 (2005).
93. G. D. Dakubo *et al.*, Control of glial precursor cell development in the mouse optic nerve by sonic hedgehog from retinal ganglion cells. *Brain Res.* **1228**, 27–42 (2008).
94. C. I. Ugbo, I. Smith, B. J. Whalley, W. D. Hirst, M. Rattray, Sonic hedgehog signalling mediates astrocyte crosstalk with neurons to confer neuroprotection. *J. Neurochem.* **142**, 429–443 (2017).
95. P. G. Fuerst *et al.*, DSCAM and DSCAML1 function in self-avoidance in multiple cell types in the developing mouse retina. *Neuron* **64**, 484–497 (2009).
96. S. Hrvatin *et al.*, Single-cell analysis of experience-dependent transcriptomic states in the mouse visual cortex. *Nat. Neurosci.* **21**, 120–129 (2018).
97. F. M. Krienet *et al.*, Innovations in primate interneuron repertoire. bioRxiv:10.1101/709501 (23 July 2019).
98. J. W. Phillips *et al.*, A repeated molecular architecture across thalamic pathways. *Nat. Neurosci.* **22**, 1925–1935 (2019).
99. G. I. Botchkina, L. P. Morin, Specialized neuronal and glial contributions to development of the hamster lateral geniculate complex and circadian visual system. *J. Neurosci.* **15**, 190–201 (1995).
100. J. Su, K. Gorse, F. Ramirez, M. A. Fox, Collagen XIX is expressed by interneurons and contributes to the formation of hippocampal synapses. *J. Comp. Neurol.* **518**, 229–253 (2010).